Journal of Power Sources 196 (2011) 4102–4108

Contents lists available at ScienceDirect

Journal of Power Sources

journal homepage: www.elsevier.com/locate/jpowsour

Graphene-conducting polymer nanocomposite as novel electrode for supercapacitors

Humberto Gómez [a,e], Manoj K. Ram [b,c,*], Farah. Alvi [a], P. Villalba [d,e], Elias (Lee) Stefanakos [c], Ashok Kumar [a,b]

[a] Department of Mechanical Engineering, University of South Florida, Tampa, FL, USA
[b] Nanotechnology Research and Education Center (NREC), University of South Florida, Tampa, FL, USA
[c] Clean Energy Research Center (CERC), University of South Florida, Tampa, FL, USA
[d] Department of Chemical and Biomedical Engineering, University of South Florida, Tampa, FL, USA
[e] Universidad del Norte, Departamento de Ingenieria Mecanica, Barranquilla, Colombia

ARTICLE INFO

Article history:
Received 14 September 2010
Received in revised form 30 October 2010
Accepted 1 November 2010
Available online 9 November 2010

Keywords:
Conducting polymers
Batteries
Polyaniline
Graphene
Supercapacitors

ABSTRACT

A novel graphene–polyaniline nanocomposite material synthesized using chemical precipitation technique is reported as an electrode for supercapacitors. The graphene (G)–polyaniline (PANI) nanocomposite film was dissolved in N-Methyl-2-pyrrolidone (NMP) and characterized using Raman, FTIR, Scanning Electron Microscopy, Transmission Electron Microscopy, and cyclic voltammetry (CV) techniques. The interesting composite structure could be observed using different ratios of graphene and aniline monomer. The supercapacitor is fabricated using G–PANI in N-Methyl-2-pyrrolidone (NMP) and G–PANI-Nafion films on graphite electrodes. A specific capacitance of 300–500 F g^{-1} at a current density of 0.1 A g^{-1} is observed over graphene–PANI nanocomposite materials. The aim of this study is to tailor the properties of the capacitors through the optimization of their components, and packaging towards a qualification for portable systems applications. Based on experimental data shown in this work, conducting polymer nanocomposite capacitor technology could be viable, and could also surpass existing technologies when such a novel approach is used.

1. Introduction

Industry and research centers around the globe are coping to address the world-wide energy demand, and are competing with all available alternate technologies. Supercapacitors represent an attractive alternative for portable electronics and automotive applications due to their high specific power and extended life. In fact, the growing demand of portable systems and hybrid electric vehicles, memory protection in CMOS, logic circuit, VCRs, CD players, PCs, UPS in security alarm systems, remote sensing, smoke detectors, etc. require high power in short-term pulses [1–8]. So, in the last 20 years, electrochemical capacitors have been required for the development of large and small devices driven by electrical power [9–11]. The worldwide market for supercapacitors in 1999 was about US $115 million covered by low-voltage devices, and in 2010 the global market is about US $50 billion for batteries [12]. Recently, the double layered high performance supercapacitors based on activated carbon have been marketed [13]. We know that supercapacitors are well compared to the secondary battery which exhibits faster and higher power capability, long life, wide thermal operating range, and is cost effective in the maintenance of the power devices [14]. The supercapacitors have been made using highly conductive, lightweight polymers such as polyanilines (PANIs), polypyrroles, and polythiophenes [15,16]. However, high power supercapacitors are a challenge to build using conducting polymer because the conducting polymers exhibit poor stabilities during the charge/discharge process. The activated carbon and carbon nanotubes (CNTs), in recent days, have been used to fabricate supercapacitors due to their good stability but these microstructures limit the value of the capacitance. The CNT-PANI has been tested in supercapacitor electrodes and high capacitances, improving the PANI stability as well [17,18]. However, the use of CNTs has been restricted from achieving electric double-layered capacitance for active devices. The two-dimensional (2D) honeycomb lattice structure of graphene has exhibited unusual and intriguing physical, chemical and mechanical properties [19]. The graphene–polyaniline (G–PANI) composite material has recently been used for energy application [20–24]. As the result of the high quality of the sp^2 carbon lattice, electrons have been found to move ballistically in the graphene layer, even at ambient temperatures. In

* Corresponding author at: Nanotechnology Research and Education Center (NREC), University of South Florida, 4202 E Fowler Ave., ENB 118, 33620, United States. Tel.: +1 813 974 3942; fax: +1 813 974 3610.
E-mail address: mkram@usf.edu (M.K. Ram).

0378-7753/$ – see front matter © 2010 Elsevier B.V. All rights reserved.
doi:10.1016/j.jpowsour.2010.11.002

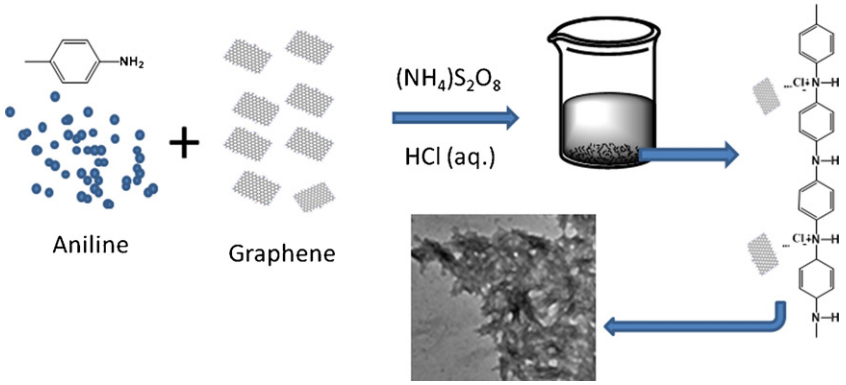

Fig. 1. Schematic of G–PANI synthesis.

this work, the nanocomposite formation of graphene is produced in order to understand how the graphene could be exploited for energy application [25]. The G–PANI has been synthesized using graphene platelets which have been successfully applied in conjunction with an aniline monomer to produce highly conductive nanocomposite material.

In this work, G–PANI nanocomposites are prepared using different molar ratios of aniline and graphene by the wet polymerization method using commercial graphene platelets. The present study shows the characterization of the supercapacitor application of G–PANI films characterized by Raman spectroscopy, FTIR, cyclic voltammetry, impedance, Scanning Electron Microscopy (SEM), Transmission Electron Microscopy (TEM) techniques, respectively. The specific capacitances have been determined for G–PANI materials in different electrolytic media.

2. Experimental

2.1. Reagents and materials

Aniline (99.5%), ammonium persulfate (98%), sodium hydroxide (powder, 97%) and hydrochloric acid (37%) were all ACS grade and purchased from Sigma–Aldrich (USA). N-N-dimethyl formamide (99.8%) was purchased from Alfa Aesar (USA) and graphene platelets (less than 10 nm in thickness) were purchased from Angstrom Materials (USA). All these chemicals and materials were employed as purchased without any further purification unless specified.

2.2. Synthesis and characterization of the graphene–polyaniline nanocomposite conducting polymer

The G–PANI nanocomposite was chemically synthesized by oxidative polymerization of aniline using ammonium peroxydisulfate $[(NH_4)_2S_2O_8)]$ under controlled conditions. The aniline to graphene ratio was kept at 1:1 and 1:2 ratios, and added in 1 M HCl solution, where the solution was cooled to 4 °C in an ice bath. Ammonium peroxydisulfate (0.025 M) was also dissolved in 200 mL of 1 M HCl solution, and the solution was pre-cooled to 4 °C. Later, $[(NH_4)_2S_2O_8)]$ in 1 M HCl solution was added slowly in the aniline solution, and the reaction was continued for 12 h. The dark green precipitate of the G–PANI nanocomposites recovered from the reaction vessel was filtered, and washed using deionized water, methanol, acetone, and diethyl ether for the elimination of the low molecular weight polymer and oligomers. Further, this precipitate was heated at 100 °C in a temperature-controlled oven [26]. The schematic of synthesis process is shown in Fig. 1.

2.3. Optical characterizations of films

G–PANI nanocomposites were deposited on Si (1 0 0) wafers and doped in 1.0 M HCl. The G–PANI film was characterized for its different vibrational bands by Fourier transform infrared (FTIR) spectrophotometer. The sample chamber of the spectrophotometer was continuously purged with nitrogen for 15–20 min prior to data collection and during the measurements for the elimination of the water vapor absorption. For each sample, 8 interferograms were recorded, averaged and Fourier-transformed to produce a spectrum with a nominal resolution of 4 cm. Finally, the FTIR spectra of G–PANI nanocomposite films were obtained after proper subtraction to a substrate silicon base line. Raman studies of G–PANI deposited on Si were conducted to derive information regarding the Raman Shift and absorption bands of inter- and/or intra-gap states.

2.4. Surface/structure characterization

The surface morphology and the size of G–PANI films were then investigated by Field Emission Scanning Electron Microscopy (FESEM). Following, the crystalline structure of the G–PANI nanocomposite was investigated using high-resolution transmission electron microscopy (HRTEM).

2.5. The electrode material

Polymer nanocomposite materials typically have the characteristics of both components and can energetically accommodate dopant ions in a more efficient way. The capacitance study was made by mixing the G–PANI with nafion and dried over a graphite electrode. Further, the capacitance was also studied in N-methyl-2-pyrrolidone (NMP) cast G–PANI films coated over the graphite electrode. The G–PANI films of various thicknesses were fabricated using the spin coat and solution cast techniques and then dried at 100 °C. The above mentioned G–PANI film can be deposited with high conductivity on various conductive substrates, with the best characteristics being obtained on platinum, gold, indium tin oxide (ITO), and graphite.

3. Results and discussion

Fig. 2a and b shows the SEM picture of undoped G–PANI films made using NMP on Silicon substrate, illustrating the interesting structure of an interpenetrating network throughout the G–PANI surface. The graphene flake structure on the surface of G–PANI cannot be observed because the film is made using NMP. The NMP works as plasticizer which produces a smooth film. This film was doped using 0.2 M HCl for couple of minutes; care must be taken

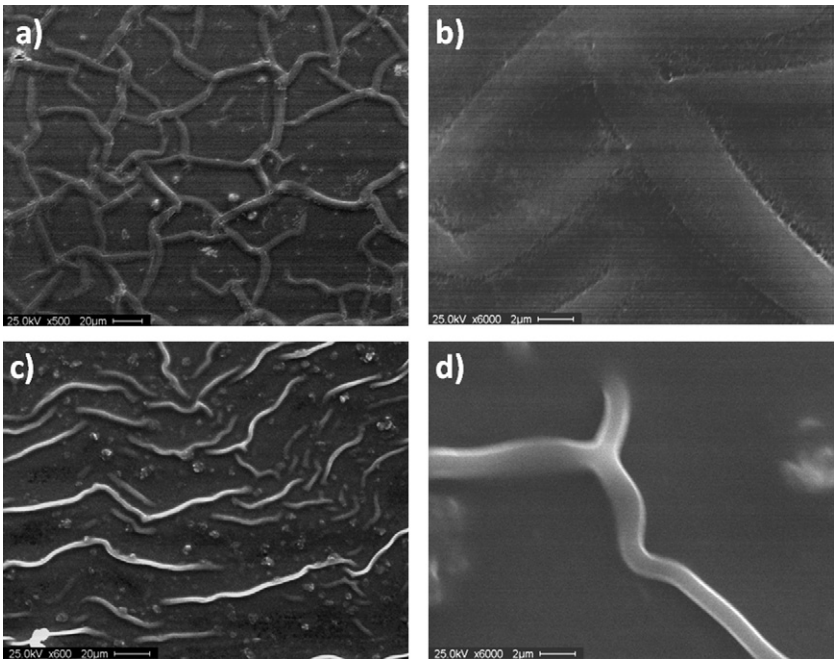

Fig. 2. SEM micrograph G–PANI undoped (a and b) and G–PANI doped in 0.2 M HCl films (c and d).

as not to leave the film in the HCl, otherwise, leaching of the film occurs from the Si substrate. Fig. 2c and d depicts the HCl doped NMP–G–PANI film. The doped graphene PANI film shows the less lined penetrating structure because doping changes the total morphology of polyaniline due to the creation of polaron and bipolaron structure throughout the chain [27]. Fig. 3a depicts the structure of the graphene platelets used for the synthesis and Fig. 3b shows the TEM picture of G–PANI nanocomposite film. Fig. 3c reveals an interesting structure where graphene flakes can be seen embedded in the polyaniline suggesting a graphene interconnection with the polymer network. Fig. 4 shows the FTIR spectra of G–PANI (undoped) deposited on silicon with characteristic bands at 3907, 3693, 3410, 3341, 3095, 2590, 1963, 1668, 1596, 1514, 1429, 1319, 1274, 1171, 1151, 1008, 858, 759, and 546 cm^{-1}. Among these, the band at 3410 cm^{-1} is due to the N–H stretching of PANI in graphene–PANI (undoped). The appearance of peaks at 1596 and 1514 cm^{-1} are attributed to the C=C stretching of the quininoid and benzenoid rings, respectively. The band at 1319 cm^{-1} is assigned to the emeraldine base structure. Further, the band at 1171 cm^{-1} is due to the N=Q=N, where Q represents the quininoid ring. The characteristic bands of graphene for C=O and C–C are shifted to 1668 cm^{-1} and 1008 cm^{-1} due to the presence of polyaniline in the G–PANI nanocomposite material.

Fig. 5 shows the Raman spectroscopy of the G–PANI-1 (1:1 ratio) and G–PANI-2 (1:2), nanocomposite systems deposited on silicon substrates. The Raman spectra shows bands at 1136, 1164, 1192,1197, 1221, 1244, 1286, 1346, 1375, 1417, 1438, 1494, 1520, 1583, 1614, and 1632 cm^{-1}, and is a complementary technique to FTIR for the identification of vibrational modes at the surface of carbon based materials. The broad asymmetric bands at 1500–1700 cm^{-1} are very characteristic of polyaniline system. The Raman bands at 1583 and 1346 cm^{-1} are due to D peaks and

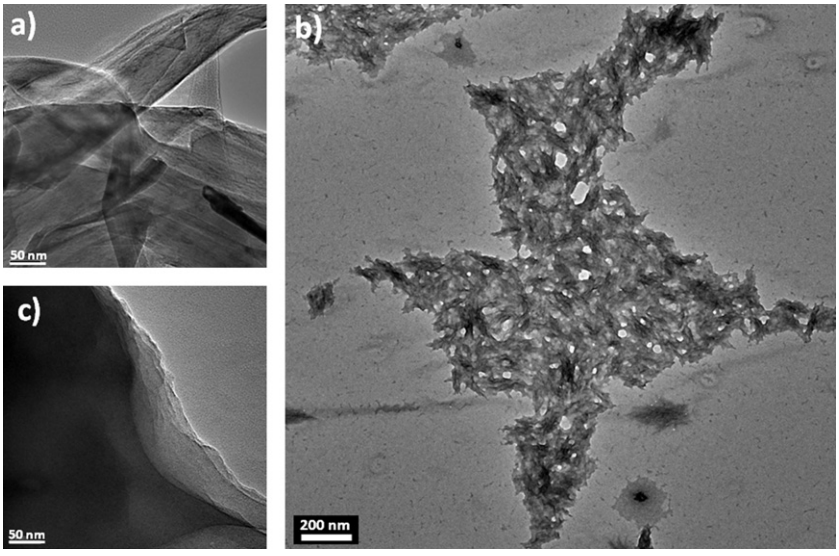

Fig. 3. TEM picture of the graphene platelets used for the synthesis (a), the G–PANI-nanocomposite film structure (b), and their resulting interaction in the polymer nanocomposite network (c).

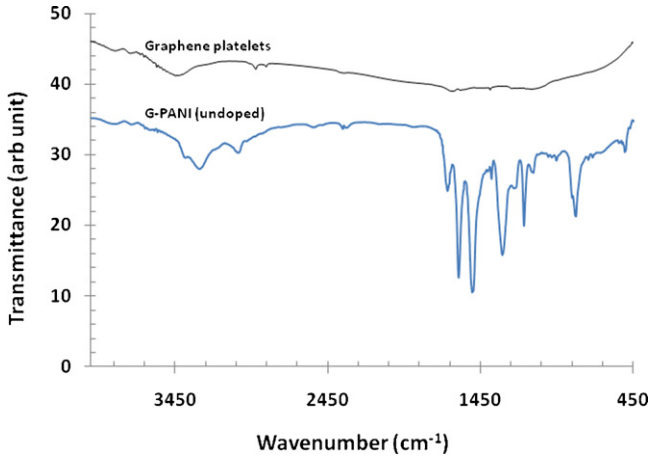

Fig. 4. FTIR spectra of graphene–polyaniline films.

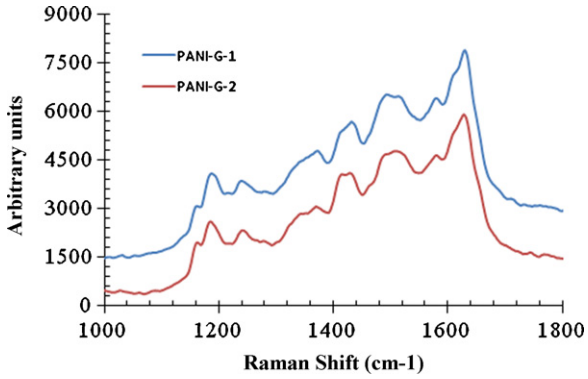

Fig. 5. Raman studies on graphene–polyaniline nanocompsosite at two different monomer:graphene ratio.

G peaks, respectively, indicative of the lattice distortions of the graphene due to the presence of the polyaniline in the network. The peak at 1375 cm^{-1} present in G–PANI structure reveals that graphene does not only make the nano-composite material, but also could be acting as a dopant in the nanostructure.

Cyclic voltammetry (CV) of graphene dissolved in N-N-dimethylformamide (DMF) and deposited on ITO plate was performed in 0.1 M camphor sulfonic acid and 2 M H_2SO_4, and the corresponding voltammograms. Fig. 6a shows the CV measurement as a function of scan rate (5, 10, 20, 50, and 100 mV s^{-1}). A distinct peak centered at 0.6 V corresponds to the oxidation of graphene platelets. The graphene also exhibits interesting electrochemical behaviors in a diffusion controlled system where the conductivity is induced by a charge transfer doping mechanism. Fig. 6b reveals the CVs of graphene and, shows peaks at 0.45 V (oxidation) and 0.4 V (reduction). The graphene is completely reversible in two different electrolytic systems as shown in Fig. 6a and b.

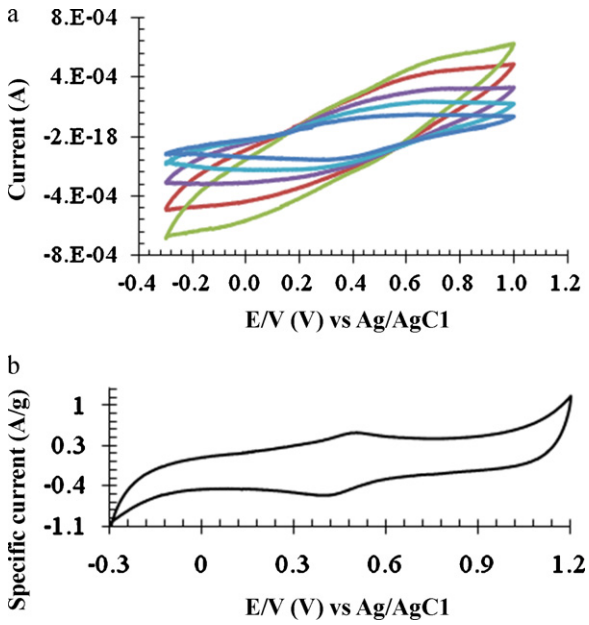

Fig. 6. Cyclic volammetry of graphene in 0.1 M camphor sulfonic acid (a) and CV of graphene in 2 M H_2SO_4 (b).

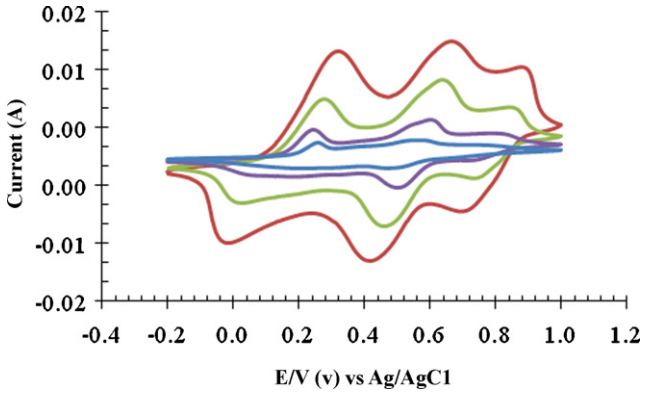

Fig. 7. Cyclic volammetry of G–PANI in 0.2 M HCl.

Fig. 7 shows the CV of G–PANI films vs. Ag/AgCl as a function of scan rate (5, 10, 20, 50, and 100 mV s^{-1}) in 0.2 M HCl. It can be observed that the reversible redox system with oxidation peaks at 0.3, 0.68 and 0.92 V, and reduction peaks at 0.7, 0.42, −0.05 V, respectively. The peak centered at 0.65 V is attributed to the oxidation of emeraldine form of PANI, whereas the peak at 0.86 V is due to the pernigraniline form of PANI (otherwise known as protonation of PANI) [28]. Interestingly, from Fig. 7 it is obvious that the G–PANI nanocomposite exhibited distinct redox peaks at −0.1 V.

The square of current vs. square root of scan rate for G–PANI films in 0.1 M HCl for redox potential is linear (figure not shown).

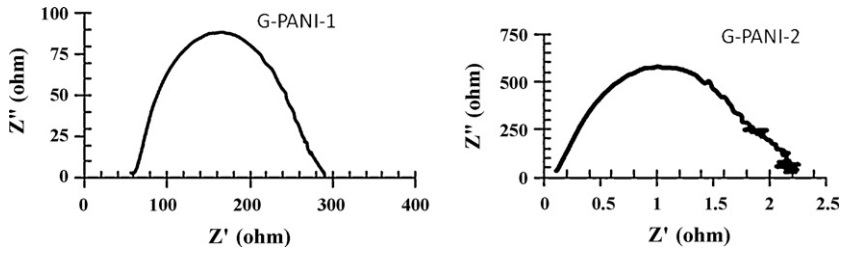

Fig. 8. Nyquist plot of graphene polyaniline at difffrent monomer:graphene ratios in 2 M H_2SO_4.

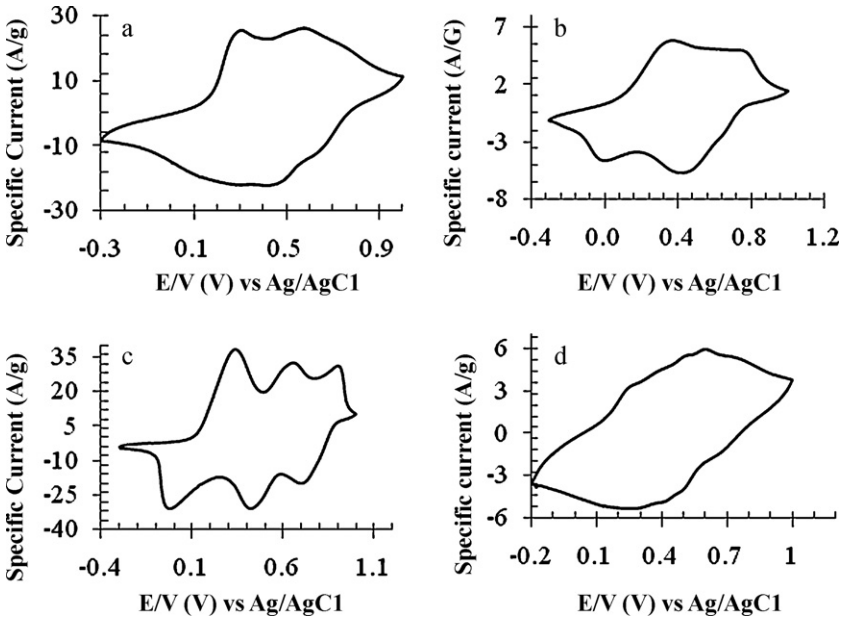

Fig. 9. Cyclic volammetry of graphene deposited on graphite substrate in 2 M H_2SO_4 (a), G–PANI films in 2 M H_2SO_4 (b), and G–PANI fabricated on a graphite electrode (c and d) using NMP and nafion, respectively.

The diffusion coefficient D_0 in HCl medium for G–PANI nanocomposite has been calculated using the Randles–Sevcik equation [29] as

$$\mathrm{Ip} = (2.687 \times 10^5) n^{3/2} \mathrm{A} D_0^{1/2} C_v^{1/2} \quad (1)$$

where n is the number of electrons transferred in the reaction, A is the electrode area, C is the concentration of the diffusing species in the bulk of the electrolyte, and v is the sweep potential rate. By using values of $n = 2$ and $C = 0.2$ M HCl, the diffusion coefficient D_0 was found to be 8.0×10^{-8} cm^2 s^{-1}. This value is more than two orders in magnitude than the polyaniline systems alone. The resistance of the supercapacitor cell is strongly dependent on the resistivity of the electrolyte used and the size of the ions from the electrolyte that diffuses into and out of the G–PANI films.

Fig. 8 shows the Nyquist plots of the capacitor just based on G–PANI films made at two different ratios in 2 M H_2SO_4. It shows the highly conducting graphene–PANI film. The semicircle observed in different ratios in 2 M H_2SO_4 are indicative that the systems are diffusion controlled. The resistance of the films at 2 M H_2SO_4 has been found to be 56 Ω and 0.1 Ω, respectively. The lower resistance is indicative that graphene makes a very highly conductive film in 2 M H_2SO_4 and has higher capacitance values.

The potential of using these composites as electrode materials for supercapacitors are tested by standard cyclic voltammetry (CV) and galvanostatic charge–discharge techniques. All electrochemistry measurements were conducted in a three-electrode cell, using a working electrode prepared by casting a nafion-impregnated G–PANI nanocomposite sample onto a graphite electrode, a platinum sheet used as the counter electrode, and AgCl/Ag used as the reference electrode. The electrolytes used consisted of 2 M H_2SO_4 in order to understand the charge–discharge technique in an acid media. The cyclability of this graphene-conducting polymer (PANI) electrode is examined under long-term cycling over 100 cycles, which has shown a good cyclic performance and reversibility. After the charge transfer process, the conducting polymer is electronically conductive. In developing supercapacitors, the electrode material and electrolyte characteristics should be considered jointly. Electrochemical characteristics, such as impedance and capacitance are studied in capacitor fabrication as well. The materials must maintain their high conductivity at all times throughout the various redox processes taking place during charge/discharge cycles. This is important, particularly during discharge for longer periods of time, so the material can get closer to the ideal situation of having a battery-like energy density while maintaining the high capacitor-like power density. Fig. 9a shows the CV of graphene deposited on graphite substrate in 2 M H_2SO_4 as the working electrode, Ag/AgCl as reference, and Pt as a counter electrode. Fig. 9b shows the CV of G–PANI films in 2 M H_2SO_4. Fig. 9c and d shows

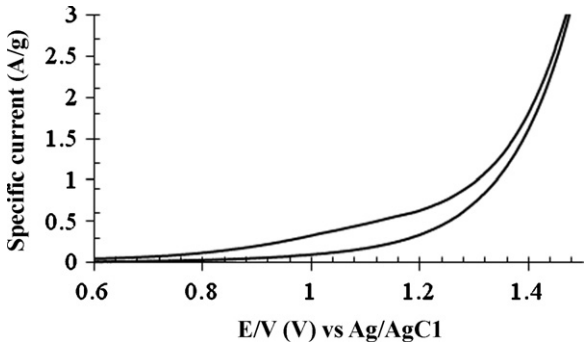

Fig. 10. Cyclic volammetry of G–PANI-2 films (1:2 ratio) in 2 M KOH.

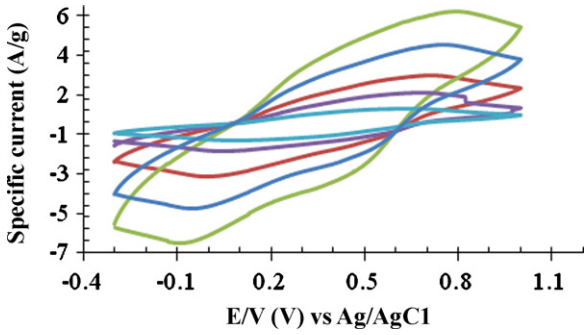

Fig. 11. Cyclic volammetry of G–PANI-2 films (1:2 ratio) in nafion-in 2 M HCl.

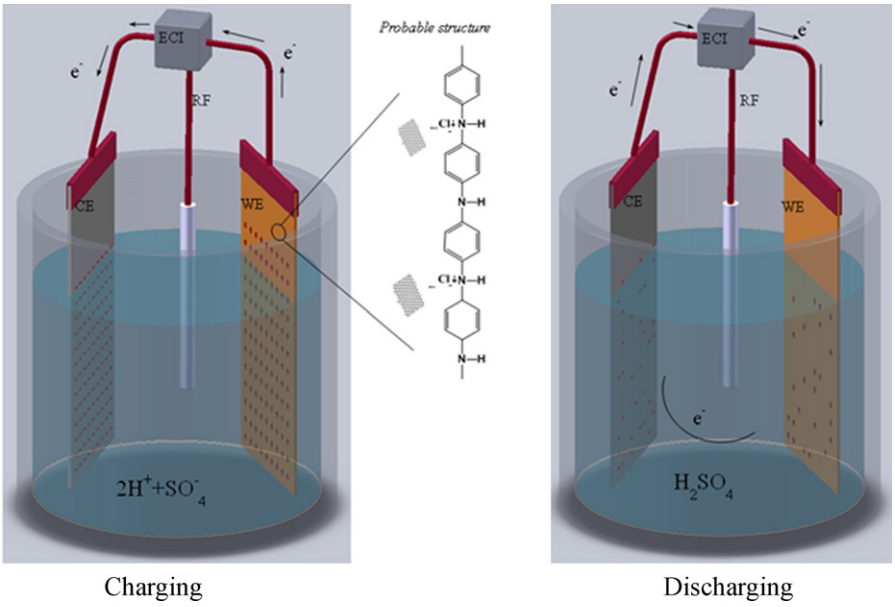

Fig. 12. Schematic of charging and discharging mechanism using G–PANI-2 (1:2 ratio) electrode in 2 M H_2SO_4 electrolyte in the electrochemical cell.

the CV of G–PANI fabricated on a graphite electrode using NMP and nafion, respectively. It is interesting to observe that the CV behavior of G–PANI film obtained on graphite substrate at different binders (NMP and nafion) differ in 2 M H_2SO_4 electrolytic system. It is also remarkable to note that the G–PANI composite retains the characteristic features of CV for around 100 cyclic, and further it shows fewer features (figure not shown). The behavior of the CV could also be interpreted due to removal of oxygen containing group from PANI systems. The CV obtained for H_2SO_4 shows the better reversibility in the systems.

To further understand the effect of acid and basic electrolytic over the value, the CV on G–PANI films was studied in 2 M KOH solution. Fig. 10 shows the CV of G–PANI-2 in 2 M KOH to understand the capacitance effect. It did not reveal the redox characteristics CV in the KOH system due to the undoped state, which prolonged in the KOH electrolyte. So, it is indicative that the salt or acidic systems should only be taken for the G–PANI or conducting polymer system based material for supercapacitor or rechargeable energy applications.

Fig. 11 shows the CV of G–PANI-2 in nafion system as a function of scan rate in 2 M HCl. The CVs show the diffusion controlled system. The CV study is indicative that nafion is a good binder similar to N-Methyl-2-pyrrolidone (NMP) for G-PANI nanocomposite material.

Fig. 12 shows the schematic of charging and discharging using G–PANI-2 electrode in 2 M H_2SO_4 electrolyte in the electrochemical cell. The specific capacitance is obtained by studying the equation $C = -1/2\pi fZ''$ [30], where Z'' is the imaginary part of the total complex impedance. The single electrode specific capacitance values were evaluated by multiplying the overall capacitance by a factor of two and divided by the mass of a single electrode material. We have also obtained the capacitance values by using the equation $C = i/s$ where 'i' is the current and 's' is scan rate. The charge–discharge characteristics of the capacitor cells are evaluated at a constant current.

The discharge capacitance 'Cd' is evaluated from the linear part of the discharge curves using the relation. $Cd = i\Delta t/\Delta V$ where 'i' is the constant current and 'Δt' is the time interval for the voltage change of ΔV.

The columbic efficiency 'η' was nearly 1.2 calculated using (η = charging time/discharging time × 100%) in Figs. 13 and 14 for

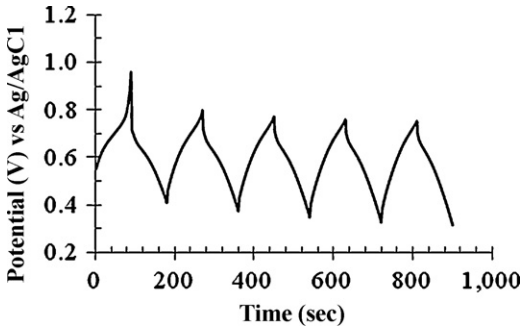

Fig. 13. Charging and discharging of G–PANI-2 in 0.2 M TBATFB.

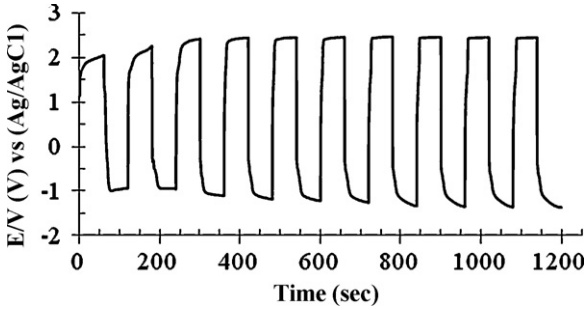

Fig. 14. Charging and discharging of G–PANI-2 in 2 M H_2SO_4.

the G–PANI nanocomposite in organic and inorganic electrolytes, respectively. The charging of G–PANI is measured in acetonitrile containing tetrabutyl ammonium tetrafluoroborate (TBATFB) as an electrolyte whereas the similar charging and discharging response have been observed for the G–PANI film studied in the 2 M H_2SO_4 (Fig. 14).

4. Conclusions

G–PANI nanocomposites have been synthesized by varying the monomer to graphene ratio for obtaining highly conducting sys-

tems suitable to supercapacitor applications. The morphology of the G–PANI has been characterized by using SEM, TEM, FTIR, and Raman to understand the graphene effect over the polyaniline network system. The presence of graphene in polyaniline shows the penetrating network like structure in G–PANI film, whereas the TEM shows how the graphene platelets are making the network structure with polyaniline. The high specific capacitance and good cyclic stability have been achieved using 1:2 aniline to graphene ratio by weight of G–PANI polymer. This result has proved that the presence of graphene in network of polyaniline changes the composite structure, and could easily be exploited for high powered supercapacitor applications for portable devices. Based on these results from G–PANI polymer nanocomposite, new synthesis applying G–polyanilines and G–polythiophenes are in progress as a future work for supercapacitor applications.

Acknowledgement

This research was partially supported by NSF CREST grant # 070734232.

References

[1] R.A. Huggins, Solid State Ionics 134 (2000) 1–29.
[2] F.I. Simjee, P.H. Chou, IEEE Trans. Power Electron. 23 (2008) 3.
[3] R. Kötz, M. Carlen, Electrochim. Acta 45 (2000) 15–16.
[4] C. Du, N. Pan, Nanotechnology 17 (2006) 5314.
[5] M. Nakamura, M. Nakanishi, K. Yamamoto, J. Power Sources 60 (1996) 225.
[6] P. Raghavana, X. Zhaoa, C. Shina, D.H. Baeka, J.W. Choia, J. Manuela, M.Y. Heoa, J.H. Ahna, C. Nahb, J. Power Sources (2010).
[7] L.Z. Fan, Y.S. Hu, J. Maier, P. Adelhelm, B. Smarsly, M. Antonietti, Adv. Funct. Mater. 17 (2007) 3083.
[8] H. Nakanishi, B.A. Grzybowski, J. Phys. Chem. Lett. 1 (2010) 9.
[9] P. Simon, Y. Gogotsi, Nat. Mater. 7 (2008) 845.
[10] M. Jayalakshmi, K. Balasubramanian, Int. J. Electrochem. Sci. 3 (2010) 1196.
[11] D. Wei, S.J. Wakeham, T.W. Ng, M.J. Thwaites, H. Brown, P. Beecher, Electrochem. Commun. 11 (2009) 2285.
[12] M. Mastragostino, C. Arbizzani, F. Soavib, J. Power Sources 97–98 (2001) 812.
[13] J.P.C. Trigueiro, R.S. Borges, R.L. Lavall, H.D.R. Calado, G.G. Silva, Nano Res. 2 (2009) 733.
[14] K. Zhang, L.L. Zhang, X.S. Zhao, Jishan Wu, Chem. Mater. 22 (2010) 4.
[15] J. Jang, Adv. Polym. Sci. 199 (2006) 189–259.
[16] E. Frackowiak, V. Khomenko, K. Jurewicz, K. Lota, F. Bguin, J. Power Sources 153 (2006) 413.
[17] Y. Zhang, X. Sun, L. Pan, H. Li, Z. Sun, C. Sun, B.K. Tay, Solid State Ionics 180 (2009) 1525.
[18] V. Gupta, N. Miura, Electrochim. Acta 52 (2006) 4.
[19] G. Wang, X. Shena, J. Yao, J. Park, Carbon 47 (2009) 8.
[20] D.-W. Wang, F. Li, J. Zhao, W. Ren, Z.-G. Chen, J. Tan, Z.-S. Wu, I. G, G.-Q. Lu, H.-M. Cheng, ACS Nano. 3 (2009) 7, doi:10.1021/nn900297m.
[21] H. Wang, Q. Hao, X. Yang, L. Lu, X. Wang, Electrochem. Commun. 11 (2009) 6.
[22] Y. Zhu, S. Murali, W. Cai, X. Li, J.W. Suk, J.R. Potts, R.S. Ruoff, Adv. Mater. 22 (2010) 35.
[23] M. Srivastava, M. Kumar, R. Singh, U.C. Agrawal, M.O. Garg, J. Sci. Ind. Res. 68 (2009) 93.
[24] M. Baibarac, P. Gómez-Romero, J. Nanosci. Nanotechnol. 6 (2006) 1.
[25] C. Bai, J. Wang, S. Jia, Y. Yang, Appl. Phys. Lett. (2010) 96.
[26] H. Gomez, M.K. Ram, F. Alvi, E. Stefanakos, A. Kumar, J. Phys. Chem. C 114 (2010) 18797–18804.
[27] A. Fattoum, M. Arous, F. Gmati, W. Dhaoui, A. Belhadj Mohamed, J. Phys. D: Appl. Phys. 40 (2007) 4347.
[28] L.H.C. Mattoso, O.N. Oliveira, R.M. Faria, S.K. Manohar, A.J. Epstein, A.G. Macdiarmid, Polym. Int. 35 (2003) 1.
[29] K.R. Prasad, N. Munichandraiah, Synth. Met. 130 (2002) 17.
[30] S.R.C. Vivechand, C.S. Rout, K.S. Subrahmanyam, A. Govindaraj, C.N.R. Rao, J. Chem. Sci. 120 (2008) 1.